# Strathprints Institutional Repository

# CFD Approach of Unburned Carbon Reduction on Pulverized Coal Boiler

Jun Li[*1], Radosław Jankowski[2], Michał Kotecki[2], Weihong Yang[1],

Dariusz Szewczyk[2], Artur Brzdekiewicz[3], Wlodzimierz Blasiak[1]

[1]Division of Energy and Furnace Technology, Royal Institute of Technology (KTH)

Brinellvägen 23, SE 10044, Stockholm, Sweden.

[2] ICS Industrial Combustion Systems Limited Company, Poznan, Poland

[3]Remak-Rozruch S.A., Opole, Poland

## Abstract

Low-NOx technologies are widely used in pulverized coal boilers, but they usually produce high levels of carbon in the fly ash. High levels of unburned carbon represent fuel loss, so the overall boiler efficiency is reduced. Additionally, the higher carbon content affects the suitability of fly ash for cement applications. The purpose of this paper is to provide a CFD approach for unburned carbon reduction by optimizing operating conditions. In this paper, three different boiler loads were simulated: 200 MW, 170 MW, and 140 MW. The air supply system was simulated previously for preparing as precise as possible boundary conditions. At last, unburned carbon level of every burner was investigated, and the effects of residue residence time and the local fuel-air momentum ratio are discussed in detail. According to the predicted results, operating conditions and the residence time of the coal particles affects the unburned carbon level in fly ash. Operating conditions plays a more significant role during the combustion process, while the residence time affects char burnout only when the burner's location is low. Therefore, it is concluded that a cost effective method could be developed for reducing the unburned carbon level in ash and correspondingly, the loss on ignition level. First, it is necessary to determine which burners are operating under poor conditions through CFD analysis. Then, the fuel air momentum ratios of those burners should be modified by changing the operating conditions, meanwhile, increasing residence time of coal particles to ensure complete combustion.

**Key words:** CFD, Pulverized coal boiler, Unburned carbon, Loss on ignition

# 1 Introduction

Coal fly ash production is expected to increase over the next few decades as a result of the world's increasing reliance on coal-fired power generation. From power plant operation perspective, excessive unburned carbon in fly ash is undesirable [1]. It represents an apparent fuel loss, so the overall plant efficiency is reduced. Moreover, higher carbon content influences the further utilization of fly ash. In the national standards set up for fly ash use in cement/concrete, the permitted concentration range of unburned carbon in fly ash is indicated by the loss on ignition (LOI) parameter.

Coal-inherent parameters, coal milling, and combustion conditions are three main factors related to unburned carbon loss [2, 3]. Coal-inherent parameters include pulverized coal properties such as heating value, apparent density and specific surface area, char yield after pyrolysis, char structure, char reactivity, ash content and composition. The coal milling system affects the particle size distribution (PSD) and the moisture remaining in the pulverized coal, and the combustion conditions covers all the operating strategies affecting boiler performance, such as the selection of the rows of burners in service, the position of the burner vanes, the fuel-air ratio, air swirling, etc. In most power plants, the mill system and coal parameters have been set at their current levels for long periods. Improving the fineness of the coal mill output using a dynamic classifier to reduce unburned carbon in ash is unfeasible, because it requires coal cleaning and optimization of the coal mills. Consequently, it is important to reduce the air/coal distribution imbalance inside the furnace, to increase the air-coal mixing rates at both burners, and to increase local oxygen availability as well as the coal particle residence time.

The greatest challenge for present-day boiler operation is to achieve both low NOx emissions and satisfactory coal burnout [1, 4]. Recently, many combustion technologies have been used to reduce NOx emissions in power plants, such as air staging and fuel staging combustion. The main concept of those low-NOx combustion technologies is to control the fuel-air ratio during the coal combustion process. Previous research confirmed low-NOx combustion are useful technologies for reducing NOx emission in power plant boilers, but are usually accompanied with the generation of high levels of carbon in the fly ash [4, 5]. One low-NOx technology, over-fire air (OFA), is widely used in power plants today. Generally, the effects of OFA on LOI emission are in overall level, because OFA ports are installed symmetrically above the burners. Therefore, it is reasonable to assume that the effect of OFA on unburned carbon levels is same for all the burners. However, in actual practice, the burners are arranged in different positions and are probably operated with varying conditions, as a result, residence time of the coal particles and the local air-coal distributions are different, which

significantly affect the unburned carbon levels of burners. Additionally, it is difficult to determine which burners are operating under poor conditions and, contributing more unburned carbon.

Computational fluid dynamics (CFD) modeling has been widely applied as a cost- and time-effective analytical tool for industrial plant development and process optimization [6]. The purpose of this paper is to provide a CFD approach for analyzing the feasibility of unburned carbon reduction in a pulverized coal boiler. CFD modeling was used to investigate the unburned carbon characteristics of each burner in order to further reduce the LOI emissions by optimizing boiler operating conditions or by boiler retrofitting.

A numerical study of unburned carbon levels in a pulverized coal boiler has been performed. To obtain the most precise numerical analysis results, a two-step simulation method was adopted: air supply system simulation followed by CFD simulation. The results of the air supply system simulation were taken as the initial and boundary conditions of the CFD simulation, which mainly included the velocity vectors and the temperatures of all the combustion air. To determine the characteristics of the unburned carbon emissions, three different loads were simulated: 200 MW, 170 MW and 140 MW. The 200 MW case was selected as the base case. The CFD models were validated, the predicted values showed good agreement with data collected in power plant. Detailed investigations concerning the overall LOI emissions, char burnout ratios, residue residence time, and local fuel-air momentum ratios were carried out. The results of the numerical analysis of unburned carbon reduction are presented in this paper.

## 2 The OP-650 pulverized-coal boiler and operating conditions

### 2.1 Case-study boiler

The case-study boiler, OP-650, was a front-wall pulverized coal boiler with maximum electricity production capacity of 220 MWe. The combustion air supply was a combination of: primary air, which was introduced with the pulverized coal; secondary air, which was introduced for combustion; OFA was introduced symmetrically above the burners' arrangement; protection air and vertical slot air, which were injected from the rear wall and front wall, respectively, as shown in Figure 1. The amount of primary air controlled the rate of combustion in the chamber. The amount of secondary air controlled efficiency. Sufficient OFA was added for the complete oxidation of any unburned or partially oxidized species originating in the combustion furnace. OFA ports were located on the rear wall, there were 10 injection nozzles. In addition, 8 vertical slots-air and 2 rows protection-air were used to protect membrane wall, ensuring that the boiler was operating within a reasonable temperature range.

3

<Figure 1>

The 24 burners were arranged in 4 rows on the front wall, with 6 burners equally spaced in each row. The burners were supplied with coal from 4 mills; each burner was marked with a sign to indicate its mill source. The detailed arrangement of the burners is shown in Figure 2. The variable, $B_{ij}$, is used to indicate the detailed position of each burner, wherein *i* represents the row number and *j* represents the column number. All 24 burners were used in the 200 MW case. But in the 170 MW and 140 MW cases, mill 1 was closed and only remaining 19 burners were used. During all the combustion processes in the three cases, the amount of pulverized coal supplied to the 12 burners located in the bottom two rows accounted for 70% of the total amount of the coal, while the amount of supplied to the upper 12 was approximately 30%.

<Figure 2>

## 2.2 Operating conditions

Three different load cases were simulated in this work: 200 MW, 170 MW and 140 MW. The proximate and ultimate analyses of coal used in these three cases are shown in Table 1. The operating conditions of this boiler, shown in Table 2, were taken from the power plant.

<Table 1>

<Table 2>

The velocity vectors of the combustion air affect the fuel-air mixing rate and combustion process inside the combustion chamber. In particular, we concern how combustion air is injected into the entire combustion system. To obtain the most precise numerical analysis results, accurate initial and boundary conditions should be provided. In this work, the air supply system simulations had been performed previously.

Solidworks software was used for the air supply system simulation to predict the velocity vectors and the temperature and pressure conditions on the inlet surfaces of boiler. A 3D model was set up, consisting of combustion air ducts, 24 burners, 10 OFA ports, and the protection channel, as shown in Figure 3. Detailed air channel information was considered, including the position and angle of the blade of each burner and OFA port. This information was collected from the control signals in local power plant. There were several assumptions: 1) steady-state conditions; 2) that the whole air

duct wall was an adiabatic wall; 3) that coal was not included coal in the primary air; 4) that k-ε turbulence model was applied [7].

<Figure 3>

The comparisons of combustion air between the predicted results and measured data are shown in Table 3. The predicted results of the air supply system simulation showed good agreement with the measured data. Although the predicted values of the protection air in the lower layer were obviously smaller than that of measured values, but the absolute values were too small to affect the distribution of combustion air. Finally, the discrepancies between the predicted values and the measured values of the total amount of combustion air were approximately 0.125%, 0.456% and 0.504% at 200 MW, 170 MW and 140 MW, respectively. In this work, the predicted results of the combustion air with swirling parameters will be taken as the initial and boundary conditions of the CFD simulation for all three cases. The side view of the velocity profiles of the primary air, secondary air, and OFA are shown in Figure 4. Furthermore, according to the results of the simulation, primary air was introduced straight into the furnace with almost no swirling. The secondary air was injected with counterclockwise swirling and the velocity magnitude increased with a decreasing burner radius. OFA was injected as a compressed flow towards the center.

<Table 3>

<Figure 4>

## 3 CFD models

The commercial software, Ansys Fluent, was used to simulate combustion, fluid and particle flow, as well as heat and mass transfer inside the furnace[8]. The full boiler geometry was modeled. The cross sectional area of furnace was 15598×8958 mm$^2$ and the height of the domain was 39453 mm, as presented in Figure 1. The mesh system consisted of 796,372 cubic cells. The mesh was refined at the location of the burners, where the ignition and most of the combustion reactions occurred. In addition, all the velocity vectors obtained from the air system simulation were input as boundary conditions in Fluent by user-defined methods.

The standard k-ε model [9] with standard wall function was used to allow for the effect of turbulent flow in the furnace. Lagrangian particle trajectories of the pulverized coal particles were calculated throughout the computational domain. The discrete ordinates (DO) radiation model was

5

used to simulate radiation heat transfer. Simulating coal combustion mainly involved the modeling of devolatilization, the homogeneous combustion of gaseous volatiles, and the heterogeneous oxidation of solid char particles [10]. The dry process, which is also important, starts with a progressive heating of the coal particle by convection and radiation. In this work, the wet combustion model was used for modeling the moisture release process during the heating stage[8].

## 3.1 Devolatilization

Because of the complexity of the reaction and products generated, the details of the kinetics of devolatilization are still unclear. Although volatile matter contains many kinds of gases, we deemed it reasonable to represent it by a single virtual material. This is because the reaction rate of the volatile matter was limited by the turbulent mixing rate of the evolved gas and oxidizer at the near-burner condition [11]. Therefore, the overall kinetics expressions commonly used in devolatilization models are shown in following overall reaction:

$$Coal(s) \rightarrow \alpha C_x H_y O_z\,(g) + \beta Char(s) + \cdots$$

In this work, two-competing-steps model is applied for devolatilization [12]. Assuming that there are two competing reactions, the first reaction has an advantage at lower temperatures while the other reaction plays dominant role at higher temperatures. The model provides the rate of volatile matter evolution and the related char and volatile yields. The two kinetic rates are weighted to yield an expression for devolatilization as [8]:

$$\frac{m_v(t)}{(1-f_{\omega,0})m_{p,0} - m_a} = \int_0^t (\alpha_1 r_1 + \alpha_2 r_2)\exp\left(-\int_0^t (r_1 + r_2)dt\right) dt$$

where $\alpha_1$ is the value of volatile matter percentage obtained from the proximate analysis of coal, and $\alpha_2$ is given the value of 0.8, and it reflects the characteristics of devolatilization at high temperatures [13]. The variables $r_1$ and $r_2$ are competing rates that control the devolatilization yields over different temperature ranges; both of these variables appear in Arrhenius expression: $r_i = A_i \exp(-E_i/RT_p)$. The detailed kinetic data for coal devolatilization are given in Table 4.

<Table 4>

## 3.2 Char burnout

6

Heterogeneous char reactions are governed by the chemical kinetic rate and the external diffusion rate of oxygen to the char surface [14]. Both diffusion and intrinsic kinetics were included in the char oxidation sub-model, in which the surface reaction rate is determined either by kinetics or by a diffusion rate. The diffusion coefficient was calculated as follows [15]:

$$D_0 = 2.53 \times 10^{-7} \frac{T_m^{0.75}}{d_p}$$

The char combustion kinetic rate was expressed with the Arrhenius form: $k_c = A_c \exp(-E_c/RT_p)$. The pre-exponential factors and the activation energy of the heterogeneous reactions were calculated with the following equations [16]:
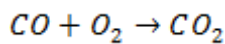
$$E_c = -24.83 + 148(\frac{C}{1 - A - M})$$

$$A_c = \exp(\ln(k_{1750}) + \frac{E_c}{1750R}) \frac{10}{P_0^{0.5}}$$

$$\ln(k_{1750}) = 2.8 - \frac{7.58C}{1 - A - M}$$

**3.3 Gaseous combustion**

The volatile matter depends on the fuel type and pyrolysis conditions; it mainly consists of gas phase hydrocarbons. Two-steps global combustion was used for the homogeneous combustion of gaseous volatiles; it involved two overall reactions as follows and calculated by the Eddy-Dissipation model [8]:

$$C_x H_y O_z(g) + \lambda O_2 \rightarrow \alpha CO + \beta CO_2 + \frac{y}{2} H_2 O$$

$$CO + O_2 \rightarrow CO_2$$

# 4 Results

**4.1 Validation**

In this paper, the predicted results of the 200MW case were compared to measured values, as shown in Table 5. It is necessary to note that there are some differences between the measured values and the predicted values due to their different positions; the measured data were only available before the air-preheater, while the predicted results were the mass-weighted-average values at the furnace exit. Despite these differences, the predicted results still show good agreement

with the measured values. According to measured data, the concentrations of $O_2$ and CO on the left side of backpass were 2.935% and 2007.2 mg/Nm$^3$, respectively and 3.329%, and 241.2 mg/Nm$^3$, respectively, on the right side. The predicted average concentrations of $O_2$ and CO were within a reasonable range, 3.3%, and 856 mg/Nm$^3$, respectively. In actual working practice, the temperature of flue gas exiting the furnace is still high enough for oxidation reactions. Therefore, a lower $O_2$ content before the air-preheater than at the furnace exit would be reasonable. However, the predicted value of CO concentration was lower than the average of the measured values, probably because the rate of oxidization of carbon in fly ash was faster than the CO consumption rate after the furnace exit; however, these results need to be confirmed.

<Table 5>

The further validation of CFD models was accomplished in this paper, as the mass fractions of unburned carbon in ash were measured during the plant test, except for the 140 MW case. The deviation of all measured values was 0.4. The final comparison between the predicted values and the measured data of the LOI are shown in Table 6. It is obvious that the predicted LOI values agreed with the measured data very well, and the coal particles achieved a more completed combustion when the boiler operated under the normal load (200 MWe) compared to lower loads conditions. Because the combustion conditions in the CFD were ideal compared to real operating conditions, the predicted LOI values were lower than that measured in both cases.  Thus, it could be concluded that the adopted numerical models in the present calculations are reasonable for combustion.

<Table 6>

**4.2 Temperature, $O_2$, and CO distributions at 200 MW**

Two different cross sections were used to examine the temperature, $O_2$, and CO distributions in the 200 MW case: a vertical section pass though the central line of burners B14, B24, B34, and B44; and a horizontal section at the furnace exit. Both sections are shown in Figure 5 and Figure 6. In Figure 5, a relatively high temperature of flue gas is seen in the middle of the furnace and near the rear wall. Super-heaters were not considered in this simulation work, so the temperature of the flue gas is higher than the normal level at furnace exit. The $O_2$ of the air injected into the furnace was quickly consumed during the combustion reactions, because the temperature inside the furnace was

high enough to oxidize the volatile matter and char of the coal particles. It is evident that a fuel-rich environment was formed in the lower furnace region, which is beneficial in the reduction of thermal NOx. The CO concentration at the furnace exit was important in determining the combustion efficiency of the furnace; a lower CO concentration always represents good combustion in the boiler. In Figure 6, it can be seen that the CO concentration on the right side was lower than on the left side of furnace exit. Similarly, measured data in the 200 MW case showed same trend: CO concentration on the right side was much lower than that on the left side (Table 5). Therefore, it is further confirmed that the adopted numerical models and the boundary conditions applies were reasonable in this work.

<Figure 5>

<Figure 6>

## 4.3 Overall LOI at different boiler loads

LOI is a key parameter that is related to both boiler combustion efficiency and ash utilization. Thus, it was studied to determine boiler combustion performance. Figure 7 shows the LOI emissions at different boiler load cases. It can be seen that the OP-650 pulverized coal boiler was operating under more suitable conditions; the average LOI values at the three loads almost fulfilled the European standard of 5% in mass. Only the predicted LOI at 140 MW and measured LOI at 170 MW were slightly higher. Currently, the biggest market for fly ash is in concrete applications, as an additive for cement. One of the criteria for such an application is that the carbon content or the LOI limit must be lower than 6% according to ASTM standard 618, and lower than 3% in market practice [17]. The ash products with LOI approximately 2.5 wt% were performed well in concrete[18]. Therefore, the LOI emission has to be less than 3% for general market demand and 2.5% LOI emission is target, as shown in Figure 7. In this work, the LOI emission was controlled and further reduced to fulfill these tight requirements, both in combustion efficiency and ash utility. The entire low-NOx system was not altered, meaning that the reduction of the LOI had to be accomplished via adjustment of the operating conditions of the burners with higher unburned carbon emissions, while maintaining a low NOx emissions level.

<Figure 7>

## 4.4 Char burnout characters

As discussed previously, LOI emissions are caused by the unburned carbon loss of each burner. However, the LOI index cannot be used to compare the performances of the different burners, because LOI is an overall parameter used to assess the ash quality and whole combustion efficiency after combustion. Additionally, it is well known that LOI figures cannot be used to make comparisons between the performances of different coals, because they depend on the original ash yield of feed coal [19]. Thus, for comparative purposes, the char burnout ratio was proposed as an indicator of the char burnout ability of each burner. The char burnout ratio can be an indicator of the combustion efficiency, because volatile matter from coal devolatilization is combusted completely inside the furnace in all three scenarios, assuming clean wall conditions in the furnace. The char burnout ratio was calculated using the following equation [20, 21]:

$$\psi = [1 - (A/\omega_A)]/(1 - A)$$

where $\omega_A$ is the ash weight fraction in fly ash. And the relationship between LOI and char burnout ratio is as follows:

$$\psi = 1 - \frac{LOI \cdot A}{(1 - LOI) \cdot C}$$

The char content of coal is determined by the coal proximate analysis parameters, while char content of ash is affected by combustion conditions, such as the fuel-air ratio, particle diameters, residence time, and so on. Therefore, the mass flow rates of the total char injected into the boiler via each burner are easy to calculate based on the coal feed rate and char content of coal. The total char could only comprise two final forms after combustion, unburned and burnout. Unburned char from all 24 burners determined the overall unburned carbon level (LOI), while burnout char was combusted completely inside boiler.

The mass flow rates of the total char and the char burnout ratio of each burner at the three different loads are shown in Figures 8-10, in which the unburned char and burnout char are also presented separately. In Figure 8, it can be seen that burners B21, B22 and B23 operated under poor conditions, indicated by the lower combustion efficiencies compared to other burners in the 200 MW load case. Thus, most of the unburned carbon came from those three burners. The char burnout ratios of burners B21, B22 and B23 were 95.2%, 87.6% and 91.4%, respectively. In Figure 9, burners B21, B22, B31, B32, B41, and B42 were operating under poor conditions, also exhibiting lower combustion efficiencies compared to the other burners in the 170 MW load case. Likewise, those burners contributed more unburned carbon. All the char burnout ratios of those burners were below 95%. Finally, in Figure 10, burners B21, B22, B31, B32, and B41 were operating under poor conditions and, exhibiting lower combustion efficiencies compared to the other burners in the 140 MW load

case. Thus, according to Figures 8-10, it can be concluded that the burners on the left side of the boiler contributed most of unburned carbon, specifically, burners B21, B22, B31, B32, B41 and B42.

<Figure 8>

<Figure 9>

<Figure 10>

## 5 Discussion

### 5.1 Coal-inherent parameters and particle size distribution

To clearly explain the correlation between the unburned carbon and coal-inherent parameters and particle size distributions, the global reactivity of char particles, $r_g$, defined by R.H. hurt is employed [4]:

$$r_g = P_s S^{1/2} (k_i/v)^{1/2} (m_c/V_p)^{1/2} D_{eff}^{1/2}$$

Where internal surface area $S$, intrinsic reaction rate coefficient $k_i$ and carbon availability $m_c/V_p$ are determined by coal-inherent parameters as well as particle size distributions.

According to Table 1, the coal parameters used in the three load cases were very similar: lower moisture contents, higher ash contents, similar volatile contents, and comparable heat values. Additionally, because the same milling system was used, the particle size distributions of the coals in the three scenarios were almost the same as well, as shown in Figure 11, in which $Y_d$ is the mass fraction of particles with diameters greater than the particle size. In addition, it is should be noted that all the information on the operating conditions of the three cases was collected in 3 days, and the same raw coals were supplied during this testing period; thus, the slight differences were perhaps caused by deviations in sampling and analysis procedures. Consequently, the coal-inherent parameters and particle size distributions have negligible effects on the unburned carbon level of each burner. This means that the emission characteristics of unburned carbon in the three scenarios are comparable.

<Figure 11>

11

## 5.2 Effects of residence time

The requirements for complete combustion are temperature, time, and turbulence (3T)[22]. Residence time can be identified as the factor that limits the burnout quality the most, especially for a pulverized coal boiler, because its operating temperature is high (above 1000 °C). Moreover, residence time and turbulence are always considered together; the more turbulence inside furnace, the longer the residence time of the coal particles. For front-wall pulverized coal boiler, burner location also has strong effect on the residence time of the coal particles.

In order to obtain the effect of burner locations on residence time of coal particles, the average residence time of coal particles for each burner was adopted, which was calculated as:

$$t_{avg} = \frac{\sum_{i=1}^{n} t_{pi}}{n}$$

where, n is equal to 800, meaning that there were 800 coal particles from each burner injected into the combustion chamber in the CFD models. The size of the 800 coal particles followed the Rosin-rammler distribution. Details of the average residence time of the coal particles of the three different cases are shown in Figure 12. It is obvious that the residence time depended strongly on the height of the burner; the residence time decreased with increasing height of burner positions in all three load cases. The average residence time of the coal particles injected from the bottom burners are longer than that of the top burners, mainly because the coal particles must travel farther before escaping furnace, thus increasing the chances of collision among coal particles. Additionally, the residence time of the coal particles increased gradually with decreasing burner loads, which means that the residual residence time when the boiler operated at 140 MW was longer than that of the 170 MW and 200 MW load cases. Furthermore, these results show that the discrepancies in the residual residence time decreased gradually with increasing burner position. As a result, the longest residence time of the coal particles occurred in the bottom burners in the 140 MW case, which means that the coal particles injected from those burners could be combusted more completely if operated under the same conditions. However, the combustion process is not only affected by residence time, but also operating conditions such as the fuel-air momentum ratio.

**<Figure 12>**

## 5.3 Effects of operating conditions

According to the equation of the global reactivity of the char particles (see Section 5.1), the oxygen partial pressure, stoichiometric factor, and effective diffusivity in porous media also affect

12

char burnout. These factors are mostly determined by the initial operating conditions. It is well known that the swirling of combustion air mainly affects the fuel-air mixing and combustion process [23]; thus, air swirling influences flame stabilization, the residual residence time, the char combustion process, and pollutant formation. Hence, the initial fuel-air mixing is an important indicator of the unburned carbon level in fly ash. The fuel-air momentum flux ratio, defined as $MR = \rho_F v_F^2 / \rho_A v_A^2$, has been employed widely to assess the flow and combustion characteristics of a burner [23-26]. As discussed earlier, burners B21, B22, B31, B32, B41, and B42 were operating under poor conditions, thus contributing most of the unburned carbon.

To understand the effect of the operating conditions on the unburned carbon level, those 6 burners were examined. For each burner, the char burnout ratios and other combustion characteristics at different boiler loads were comparable, as it has same geometry and location. Comparisons of the char burnout ratio and the momentum ratio of those 6 burners at different boiler loads are shown in Figure 13.

<Figure 13>

Figure 13 shows that the momentum ratio strongly influences the char burnout ratio; a low initial fuel-air momentum ratio always corresponds to high char burnout ratio, because more $O_2$ is available in this condition for char complete combustion. The effects of the momentum ratio on char burnout were very clear, particularly in burners B31, B32, B41 and B42, despite longer residence time of the coal particles at the lower boiler loads. The different residence time possibly results from the unclear influence of the momentum ratio on char burnout in burners B21 and B22, and especially in burner B22, because the coal residual was allowed more time to combust before escaping the furnace in the 140 MW and 170 MW cases. Additionally, as discussed before, the lower the burner's location, the bigger the differences in the residual residence time among the three boiler loads. Thus, the residence time had a more significant effect on unburned carbon in B21 and B22, as those were the lowest burners in the 6 burners studied. In conclusion, both the fuel-air momentum ratio and the residual residence time affect char burnout, with the momentum ratio playing a dominant role. Among all the burners, the lower the initial momentum ratio, the greater the completion of char combustion, thus the lower the amount of unburned carbon left behind. Furthermore, the residence time has a greater effect on char burnout only when the burner's location is low, so that the residual residence time is much longer.

# 6 Conclusions

To further reduce LOI emissions by optimizing boiler operating conditions or by boiler retrofitting, the unburned carbon characteristics of each burner were investigated. The effects of residue residence time and local fuel-air ratio were also analyzed. Three different loads were simulated: 200MW, 170MW and 140MW. A two-step simulation method, that is, air supply system simulation and CFD simulation, was adopted so that more precise boundary conditions could be applied. The overall LOI emissions and char burnout ratios of each burner were studied. According to the predicted results, the operating conditions and the residence time of the coal particles affect the final unburned carbon level in fly ash. Operating conditions played a more significant role during the combustion process, while the residence time affected char burnout only when the burner was located at low level. Therefore, it can be concluded that a cost effective method could be developed for the reduction of unburned carbon levels in ash, and thus LOI emissions. First of all, it would be necessary to determine the burners operating under poor conditions using CFD analysis. Then, the fuel air momentum ratios of those burners could be modified by changing those operating conditions to increase residence time of the coal particles to ensure complete combustion.

# 7 Acknowledgements

# 8 Nomenclature

| | |
|---|---|
| $A$ | proximate analysis ash content in coal (wt%) |
| $A_c$ | pre-exponential factor, (kg/m$^2$ Pa s) |
| $A_i$ | pre-exponential factor (kg/m$^2$ Pa s) |
| $B_{ij}$ | position indicator of each burner, $i$ represents the row number, and $j$ |
| $C$ | proximate analysis char content in coal (wt%) |
| $d_p$ | particle diameter (μm) |
| $D_0$ | diffusion rate coefficient (m$^2$/s) |
| $D_{eff}$ | effective diffusivity in porous media |
| $E_c$ | the activation energy of char oxidation (J/kmol) |
| $E_i$ | activation energy of coal devolatilization(J/kmol) |
| $K_{1750}$ | chemical rate coefficient at temperature of 1750K (kg/m$^2$ Pa s) |
| $k_c$ | kinetic rate coefficient of char combustion (kg/m$^2$ Pa s) |
| $k_i$ | intrinsic reaction rate coefficient (kg/m$^2$ Pa s) |

| $m_a$ | ash mass in the coal particle (kg) |
|---|---|
| $m_c$ | mass of carbonaceous solid (kg) |
| $m_v(t)$ | volatile yield up to time (kg) |
| $m_{p,0}$ | initial particle mass at injection (kg) |
| | |
| $M$ | moisture content in raw coal(wt%) |
| $n$ | The total amount of coal particles |
| $P_0$ | pressure of atmosphere (Pa); |
| $P_s$ | oxygen partial pressure at particle surface (Pa); |
| $r_1$ | devolatilization rate at low temperature range (kg/m$^2$ Pa s) |
| $r_2$ | devolatilization rate at high temperature range (kg/m$^2$ Pa s) |
| $r_g$ | global reactivity of char particles (cm$^2$ /g s) |
| $R$ | gas universal constant, 8314.3 J/ (kmol·K); |
| $t_{avg}$ | average residence time of coal particles (s) |
| $t_{pi}$ | residence time of coal particle $i$ (s) |
| $T_m$ | mean particle and gas temperature (K) |
| $v$ | stoichiometric factor |
| $V$ | proximate analysis volatile content in coal (wt%) |
| $V_p$ | particle volume (m3) |
| $Y_d$ | mass fraction of particles with diameter greater than particle size |

*Greek Symbols*

| $\alpha_1$ | volatile yield factor at low temperatures |
|---|---|
| $\alpha_2$ | volatile yield factor at high temperatures |
| $\omega_A$ | ash weight fraction in fly ash(wt%) |
| $\rho_F$ | fuel density (kg/m$^3$) |
| $v_F$ | fuel velocity (Nm/s) |
| $\rho_A$ | air density (kg/m$^3$) |
| $v_A$ | air velocity (Nm/s) |
| $\psi$ | char burnout ratio |

*Abbreviations*

| LOI | Loss on ignition |
|---|---|
| CFD | Computational fluid dynamics |
| MR | fuel-air momentum flux ratio |
| PSD | particle size distribution |
| OFA | over-fire air |
| OP-650 | pulverized boiler with steam output 650 t/h |
| NA | not available |

# References

1. IEA. *Reducing carbon-in-ash*. 2010; Available from: http://www.iea-coal.org.uk/publishor/system/component_view.asp?LogDocId=82354&PhyDocID=7536.

2. Walsh, P.M., et al., *Unburned carbon loss from pulverized coal combustors.* Fuel, 1994. **73**(7): p. 1074-1081.

3. Pallarés, J., I. Arauzo, and L.I. Díez, *Numerical prediction of unburned carbon levels in large pulverized coal utility boilers.* Fuel, 2005. **84**(18): p. 2364-2371.

4. Hurt, R.H. and J.R. Gibbins, *Residual carbon from pulverized coal fired boilers: 1. Size distribution and combustion reactivity.* Fuel, 1995. **74**(4): p. 471-480.

5. Ren, F., et al., *Influence of the over-fire air angle on the flow field in a down-fired furnace determined by a cold-flow experiment.* Fuel, 2011. **90**(3): p. 997-1003.

6. Philip J, S., *Recent applications of CFD modelling in the power generation and combustion industries.* Applied Mathematical Modelling, 2002. **26**(2): p. 351-374.

7. John E. Matsson, *An Introduction to SolidWorks Flow Simulation* 2009: Schroff Development Corporation.

8. *Ansys fluent 12.0 Theory guide.* 2009.

9. Launder, B.E. and D.B. Spalding, *The numerical computation of turbulent flows.* Computer Methods in Applied Mechanics and Engineering, 1974. **3**(2): p. 269-289.

10. Smoot, L.D. and D.T. Pratt, *Pulverized-coal combustion and gasification : theory and applications for continuous flow processes / edited by L. Douglas Smoot and David T. Pratt* 1979, New York :: Plenum Press.

11. Asotani, T., et al., *Prediction of ignition behavior in a tangentially fired pulverized coal boiler using CFD.* Fuel, 2008. **87**(4-5): p. 482-490.

12. Kobayashi, H., J.B. Howard, and A.F. Sarofim, *Coal devolatilization at high temperatures.* Symposium (International) on Combustion, 1977. **16**(1): p. 411-425.

13. Li, Z.Q., F. Wei, and Y. Jin, *Numerical simulation of pulverized coal combustion and NO formation.* Chemical Engineering Science, 2003. **58**(23-24): p. 5161-5171.

14. M.A. Field, D.W.G., B.B. Morgan and P.G.W. Hawksley. *Combustion of Pulverised Coal*. in *BCURA*. 1967. London.

15. Morgan, M.E. and P.A. Roberts, *Coal combustion characterisation studies at the International Flame Research Foundation.* Fuel Processing Technology, 1987. **15**(0): p. 173-187.

16. Hurt, R.H. and R.E. Mitchell, *Unified high-temperature char combustion kinetics for a suite of coals of various rank.* Symposium (International) on Combustion, 1992. **24**(1): p. 1243-1250.

17. J. Y. Hwang, X.S., Z. Li, *Unburned Carbon from Fly Ash for Mercury Adsorption: I. Separation and Characterization of Unburned Carbon.* Minerals & Materials Characterization & Engineering, 2002. **1**(1): p. 60-39.

18. Ahmaruzzaman, M., *A review on the utilization of fly ash.* Progress in Energy and Combustion Science, 2010. **36**(3): p. 327-363.

19. Cloke, M., E. Lester, and W. Gibb, *Characterization of coal with respect to carbon burnout in p.f.-fired boilers.* Fuel, 1997. **76**(13): p. 1257-1267.

20. Costa, M., P. Silva, and J.L.T. Azevedo, *MEASUREMENTS OF GAS SPECIES, TEMPERATURE, AND CHAR BURNOUT IN A LOW-NOX PULVERIZED-COAL-FIRED UTILITY BOILER.* Combustion Science and Technology, 2003. **175**(2): p. 271-289.

21. Li, Z., et al., *Measurement of gas species, temperatures, char burnout, and wall heat fluxes in a 200-MWe lignite-fired boiler at different loads.* Applied Energy, 2010. **87**(4): p. 1217-1230.

22. Nussbaumer, T., *Combustion and Co-combustion of Biomass:  Fundamentals, Technologies, and Primary Measures for Emission Reduction†.* Energy & Fuels, 2003. **17**(6): p. 1510-1521.

23. Cheng, T.S., et al., *Effects of partial premixing on pollutant emissions in swirling methane jet flames.* Combustion and Flame, 2001. **125**(1-2): p. 865-878.

24. Coghe, A., G. Solero, and G. Scribano, *Recirculation phenomena in a natural gas swirl combustor.* Experimental Thermal and Fluid Science, 2004. **28**(7): p. 709-714.

25. Liou, T.M., L. Chen, and Y.Y. Wu, *Effects of momentum ratio on turbulent nonreacting and reacting flows in a ducted rocket combustor.* International Journal of Heat and Mass Transfer, 1993. **36**(10): p. 2589-2599.

26. Hassan, M.A., M.A. Ismail, and F.C. Lockwood, *Pulverized-coal flame stability: effect of the burner quarl cooling.* Chemical Engineering Science, 1991. **46**(10): p. 2543-2550.

## Tables

Table 1. Analysis data of pulverized coals.

|  | Units | 140 MW | 170 MW | 200 MW |
|---|---|---|---|---|
| Moisture | % | 1.53 | 1.37 | 1.43 |
| Ash | % | 23.97 | 22.87 | 24.70 |
| Volatile | % | 27.59 | 28.09 | 27.45 |
| Char | % | 46.91 | 47.68 | 46.42 |
| Lower heat value | MJ/kg | 23.447 | 23.93 | 23.147 |
| C | % | 80.54 | 80.78 | 80.41 |
| H | % | 5.26 | 5.28 | 5.30 |
| O | % | 11.06 | 10.72 | 11.12 |
| N | % | 1.71 | 1.72 | 1.69 |
| S | % | 1.43 | 1.50 | 1.48 |

Table 2. Operating conditions of the three loads.

|  | Units | 140 MW | 170 MW | 200 MW |
|---|---|---|---|---|
| Average steam | (t/h) | 403.45 | 485.86 | 581.14 |
| Pressure of main | (MPa) | 13.43 | 13.76 | 14.15 |
| Temperature of main | ($^o$C) | 536 | 538 | 538 |
| Total air flow rate | (Nm$^3$/h) | 387951 | 468756 | 553251 |
| Total coal feed rate | (t/h) | 55.11 | 65.08 | 79.15 |

Table 3. Comparisons of combustion air between the predicted results and measured data

| NO. | Name | Units | 140 MW | | 170 MW | | 200 MW | |
|---|---|---|---|---|---|---|---|---|
| | | | Predicted | Measured | Predicted | Measured | Predicted | Measured |
| 1 | Primary air | $Nm^3/h$ | 162071 | 162071 | 177012 | 177012 | 201170 | 201170 |
| | | $^oC$ | 100 | 100 | 100 | 99 | 100 | 100 |
| 2 | Secondary air | $Nm^3/h$ | 142761 | N/A | 192234 | N/A | 224810 | N/A |
| | | $^oC$ | 266 | N/A | 278 | N/A | 289 | N/A |
| 3 | Vertical slot air | $Nm^3/h$ | 24506 | N/A | 27656 | N/A | 33105 | N/A |
| | | $^oC$ | 266 | N/A | 278 | N/A | 289 | N/A |
| 4 | OFA | $Nm^3/h$ | 38299 | 36300 | 48881 | 46689 | 67865 | 65130 |
| | | $^oC$ | 266 | 265 | 278 | 278 | 289 | 289 |
| 5 | Protection air (upper layer) | $Nm^3/h$ | 12533 | 12511 | 13544 | 13369 | 16412 | 16210 |
| | | $^oC$ | 266 | 265 | 278 | 278 | 289 | 289 |
| 6 | Protection air (lower layer) | $Nm^3/h$ | 7781 | 5602 | 9430 | 6955 | 9890 | 6767 |
| | | $^oC$ | 266 | 265 | 278 | 278 | 289 | 289 |
| 7 | 2+3 | $Nm^3/h$ | 167267 | 169520 | 219890 | 222605 | 257915 | 263284 |
| 8 | 1+2+3+4+5+6 | $Nm^3/h$ | 387951 | 386004 | 468756 | 466630 | 553251 | 552561 |

Table 4.  Kinetic data of coal devolatilization.

| | Value of $i$ | $\alpha_i$ | $A_i$ ($s^{-1}$) | $E_i$ (J/kmol) | Reference |
|---|---|---|---|---|---|
| First reaction | 1 | $V$ | $3.7\times10^5$ | $7.366\times10^7$ | [13] |
| Second reaction | 2 | 0.8 | $1.46\times10^{13}$ | $2.511\times10^8$ | |

Table 5. Comparison between the predicated values and measured values.

| | Position | | $O_2$@200 MW (%, dry) | CO@200 MW (mg/$Nm^3$, dry) |
|---|---|---|---|---|
| Predicted | Furnace exit (Mass-Weight-Average) | | 3.30 | 856 |
| Measured | After air-preheater, before economizer | Left side | 2.935 | 2007.2 |
| | | Right side | 3.329 | 241.2 |
| | | Average | 3.13 | 1124 |

Table 6. Comparison between predicted and measured values of LOI.

| | Position (data processing) | 140 MW (%, wt) | 170 MW (%, wt) | 200 MW (%, wt) |
|---|---|---|---|---|
| Predicted | Outlet of domain (Mass-Weight-Average) | 5.09 | 4.85 | 3.67 |
| Measured | Fly ash (Average value of 3 samples) | NA | 5.40(±0.4) | 4.27(±0.4) |

## Figure captions

Figure 1. Geometry of OP-650 boiler for furnace simulation (all dimensions in mm)

Figure 2. Arrangement of 24 burners on Front wall (all dimensions in mm)

Figure 3. Geometry of air supply system

Figure 4. Scheme of velocity vectors of primary air, secondary air and OFA

Figure 5. Temperature, $O_2$, and CO profiles of vertical section (central line of B14, B24, B34 and B44)

Figure 6. Temperature, $O_2$, and CO profiles of horizontal section (furnace exit)

Figure 7. Overall LOI emissions of three boiler load cases

Figure 8. The mass flow rates of total char and char burnout ratio of each burner at 200MW

Figure 9. The mass flow rates of total char and char burnout ratio of each burner at 170MW

Figure 10. The mass flow rates of total char and char burnout ratio of each burner at 140MW

Figure 11. Particle size distributions of coal used in three scenarios

Figure 12. Average residence time with burner positions at three boiler loads

Figure 13. Comparison of char burnout ratios and fuel/air momentum ratios